

On the Reliability and Stability of Selective Methods in Malware Classification Tasks

Alexander Herzog*

University College London and core64
London, United Kingdom
alexander.herzog.23@ucl.ac.uk
alex@core64.co.uk

Aliai Eusebi*

University College London
London, United Kingdom
aliai.eusebi.16@ucl.ac.uk

Lorenzo Cavallaro

University College London
London, United Kingdom
l.cavallaro@ucl.ac.uk

Abstract

The performance figures of modern drift-adaptive malware classifiers appear promising, but does this translate to genuine operational reliability? The standard evaluation paradigm primarily focuses on baseline performance metrics, neglecting confidence-error alignment and operational stability. While prior works established the importance of temporal evaluation and introduced selective classification in malware classification tasks, we take a complementary direction by investigating whether malware classifiers maintain reliable and stable confidence estimates under distribution shifts and exploring the tensions between scientific advancement and practical impacts when they do not. We propose AURORA, a framework to evaluate malware classifiers based on their confidence quality and operational resilience. AURORA subjects the confidence profile of a given model to verification to assess the reliability of its estimates. Unreliable confidence estimates erode operational trust, waste valuable annotation budgets on non-informative samples for active learning, and leave error-prone instances undetected in selective classification. AURORA is further complemented by a set of metrics designed to go beyond point-in-time performance, striving towards a more holistic assessment of operational stability throughout temporal evaluation periods. The fragility we observe in SOTA frameworks across datasets of varying drift severity suggests it may be time to revisit the underlying assumptions.

CCS Concepts

• Computing methodologies → Uncertainty in AI; • Security and privacy → Robustness.

Keywords

UQ Robustness, Selective Classification, Active Learning

ACM Reference Format:

Alexander Herzog, Aliai Eusebi, and Lorenzo Cavallaro. 2026. On the Reliability and Stability of Selective Methods in Malware Classification Tasks. In *Proceedings of Make sure to enter the correct conference title from your rights*

*Both authors contributed equally to this research.

Permission to make digital or hard copies of all or part of this work for personal or classroom use is granted without fee provided that copies are not made or distributed for profit or commercial advantage and that copies bear this notice and the full citation on the first page. Copyrights for components of this work owned by others than the author(s) must be honored. Abstracting with credit is permitted. To copy otherwise, or republish, to post on servers or to redistribute to lists, requires prior specific permission and/or a fee. Request permissions from permissions@acm.org.

Conference acronym 'XX, Woodstock, NY

© 2026 Copyright held by the owner/author(s). Publication rights licensed to ACM.

ACM ISBN 978-1-4503-XXXX-X/2018/06

<https://doi.org/XXXXXXX.XXXXXXX>

confirmation email (Conference acronym 'XX). ACM, New York, NY, USA, 17 pages. <https://doi.org/XXXXXXX.XXXXXXX>

1 Introduction

Research contributions on malware classification under distribution drifts¹ has primarily centered on predictive accuracy, often treating trustworthiness as an implicit byproduct of performance. As Goodhart stated, “When a measure becomes a target, it ceases to be a good measure.” [15]

Malware classifiers experience performance degradation over time due to concept drift, caused by adversarial adaptation, the evolution of benign software, or fragile feature spaces. This violates the i.i.d. assumption upon which manually engineered or learned representations depend. Therefore, existing state-of-the-art (SOTA) drift-adaptation solutions aim to identify observations at test time that are likely to have drifted, enabling targeted mitigation. Each solution implements its own distinct detection criteria. CADE [44] calculates the minimum class-centroid distance normalized by Median Absolute Deviation; HCC [7] quantifies embedding misalignment via averaged pairwise contrastive losses between test samples and nearest training neighbors; Transcendent [5] applies conformal prediction theory to evaluate sample nonconformity relative to calibration data of the predicted class. Whether framed as confidence, nonconformity, or OOD-ness, these approaches all converge on the same aim: to attempt to produce a reliable ranking over incoming observations.

This ranking is then used in two closely related ways: (1) in selective classification, where the model abstains from predicting on drifted observations [5], or (2) in active learning, where observations are ranked by their “out-of-distribution (OOD) score” and routed to human labeling for model retraining [7, 44].² In active learning, selection follows either a threshold-based rule that annotates all samples exceeding a score threshold [44] or a budget-based rule that annotates a fixed number of top-ranked samples [7]. Selective classification prioritizes classification reliability at the cost of coverage (the proportion of accepted predictions), while active learning considers drift signals as informative for model adaptation.

Existing solutions are, however, predominantly assessed using standard performance metrics, and improvements in F1, FPR, or FNR are treated as sufficient evidence of trustworthiness under realistic conditions [32]. Crucially, offline metrics presuppose access to ground truth labels – an assumption that collapses once the model is deployed. Once released, the only signal available to assess

¹Without any loss of generality, we will refer to distribution shift and drift, and concept shift and drift, interchangeably throughout.

²Conceptually, rejected samples in selective classification are natural candidates for active learning.

decision quality is the model’s own confidence. A trustworthy system must therefore ensure that high-confidence predictions are likely correct and that low-confidence (or high OOD-score) ones are routed for further inspection. This requirement becomes most fragile under distribution shift, where modern neural networks are known to be severely miscalibrated – that is, their confidence values fail to reflect the true probability of correctness – often assigning high-confidence scores to incorrect predictions on OOD inputs [17]. Whether the goal is abstention or adaptation, the system’s behavior in deployment is therefore conditioned not by raw in-lab accuracy, but by the quality and stability of its confidence-based ranking.

The centrality of confidence-based ranking for selective classification has recently been established on firm theoretical grounds. Rabanser and Papernot [35] formalize the selective-classification gap as the discrepancy between the selective performance of a model and that of an ideal oracle that perfectly ranks predictions by correctness, and decompose this discrepancy into five contributing factors: Bayes noise, approximation error, ranking error, statistical noise, and slack due to optimization or distribution shift. Among these, ranking error is the only term that directly governs which points enter the acceptance set at any coverage level, since it reflects whether confidence scores correctly order predictions by their probability of being correct. The other terms either limit the maximum achievable accuracy or introduce estimation noise. Importantly, standard calibration, often believed to strengthen selective classifiers, cannot reduce ranking error because it preserves score ordering. Reducing the selective-classification gap therefore requires methods that actively reshape the ranking. Under distribution shift, additional slack is introduced that further destabilizes this ordering even when accuracy and calibration are controlled. These results place the quality and stability of confidence-induced ranking at the core of operational reliability under non-stationarity. This theoretical framework directly motivates our work: we measure ranking quality under non-stationary and assess whether confidence functions remain operationally reliable as data distributions evolve over time, moving beyond Rabanser and Papernot’s [35] focus on isolated shift events to sustained temporal drift.

Despite this theoretical centrality of ranking quality, confidence scoring functions are rarely subjected to direct assessment in practice. Current evaluations focus on downstream performance metrics and implicitly assume that strong F1, FPR, or FNR validates the underlying confidence function. This approach fails to differentiate whether improvements result from better ranking of predictions or from a robust model compensating for suboptimal confidence estimates. The assumption becomes particularly questionable under distribution shift, where confidence functions are most likely to be miscalibrated (refer to Figure 1 for a motivating illustration).

We propose AURORA, a framework to evaluate malware classifiers based on their confidence quality and operational resilience. AURORA subjects the confidence profile of a given model to verification using the Area Under the Risk Coverage Curve (AURC) to measure the quality of its confidence ranking [13]. We define a model’s “confidence profile” as the behavior of both (1) its OOD scoring function and (2) its vanilla confidence function. In this way, we evaluate both the reliability of a classifier’s OOD scoring function and its predictive uncertainty. The AURC quantifies how

effectively confidence scores rank instances according to their actual probability of misclassification. Intuitively, a prediction with a higher OOD score or predictive uncertainty should be more likely to be incorrect. Therefore, we expect performance to be monotonically non-decreasing when observations are rejected in order of decreasing confidence. This shows the model correctly quantifies both what samples fall outside its training distribution and when it is likely to make mistakes. If not, we are misdirecting limited annotation resources toward non-informative samples while allowing error-prone instances to remain undetected, relying on systems that do not know what they do not know.

AURORA is further complemented by a set of metrics designed to move beyond point-in-time performance, enabling assessment of operational stability across temporal evaluation periods. We focus on an abstention-based simulation that closely reflects real deployment conditions. After an initial calibration phase, we fix a rejection threshold ρ – either to satisfy a monthly annotation budget B_{M_i} [7] or to meet a target error rate [5] – and then hold this threshold constant as the data stream evolves. No additional labels are assumed to be available during this phase. Under these constraints, a reliable confidence function should lead to a stable and decision-relevant behavior: accepted samples ought to be correct with high probability, while rejected ones should concentrate the residual risk. By evaluating performance in this setting, we assess not only conventional accuracy but also the practical usefulness of the calibrated confidence signal itself over time.

With AURORA, we evaluate SOTA models across three different datasets with varying drift severity. The brittleness we uncover underscores the need for more comprehensive evaluation methodologies. Our work advances towards a more contextualized approach for examining the trustworthiness of machine learning models under realistic deployment conditions.

In summary, our contributions are as follows:

- We propose AURORA (§3), an evaluation framework that extends beyond headline performance metrics, such as F1, FNR, and FPR. AURORA introduces the use of AURC and associated Risk-Coverage curves (§3.2), as well as temporal stability metrics (§3.3), including F1 volatility ($\sigma[F1]$), Mann-Kendall trend (τ), Benefit Fraction (BF*), and rejection consistency metrics (ΔRej^* , $\sigma[Rej]^*$), to offer a holistic assessment of reliability and temporal stability in off- and online settings.
- We formalize an operational perspective where we treat models and their associated uncertainty functions as selective classifiers calibrated to meet rejection targets. Within this setting, we evaluate not only performance under rejection, but also adherence to rejection quotas and the resulting tail-risks (§3.1).
- We benchmark four SOTA solutions across three different datasets with varying drift severity. Importantly, we differentiate between learned representations and confidence functions, evaluating the latter independently of the former. We find: (1) SOTA confidence functions often under-perform a simple feed-forward network trained on the same representations (§5); (2) strong offline performance does not necessarily translate to improved reliability when classifiers are equipped with a reject option under realistic operational constraints (§5.1, §5.2); and (3) DeepDrebin [16], a

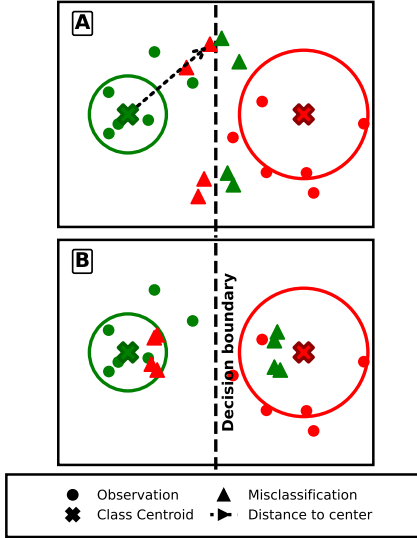


Figure 1: CADE [44] assumes that errors correlate with increased distance from cluster centers (case A). However, our evaluation with AURORA using AURC (§3.2.1), which measures the error rate as a function of coverage when samples are ranked by confidence, reveals the opposite trend. Misclassifications often occur near cluster centers (case B), placing them in regions of high confidence. This contradicts the core premise of CADE’s distance-based OOD scoring (see Figure 2 and §5). Notably, this failure is not limited to the native CADE score but also extends to softmax-based uncertainty, both of which wrongly assign high confidence to erroneous predictions. Interestingly, on some datasets, a simple MLP trained on CADE embeddings – using softmax confidence as a proxy for uncertainty – outperforms CADE’s native distance-based OOD metric. Softmax confidence declines near the decision boundary, aligning better with classifier uncertainty and offering a more reliable OOD indicator [17].

simple feed-forward network requiring only binary labels, performs comparably to or outperforms complex SOTA frameworks, which rely on additional family labels and costly training (§5.1, §5.2).

2 Motivation and Related Work

Existing Android malware detectors either optimize for stationary conditions [2, 16, 28] or aim for robustness to temporal drift [5, 7, 31, 34, 43, 44, 46, 48]. Traditional approaches rely on static or dynamic analysis to derive behavioral proxies: Drebin [2] encodes eight statically extracted feature sets (permissions, intents, API calls, etc.) as sparse multi-hot vectors; MaMaDroid [28] models package transitions via Markov chains; and APIGraph [46] embeds relational API graphs to expose functional clusters. Because hand-crafted features suffer from inherent semantic limitations and struggle to capture the novel patterns introduced by emerging threats, recent work shifts to learned representations, often realized with deep neural networks [4, 16, 19, 25, 36].

Despite advances in representation learning [48], detectors still need periodic retraining to track distribution shift [5, 7, 33]. This is

expensive: labels are scarce, yet threat volume is huge – AV-TEST logs over 450,000 new samples per day and VirusTotal more than 1 M uploads [3, 41]; manual analysis can consume four hours to six weeks per sample [45]. To stem performance decay under such constraints, SOTA systems integrate selective classification and active learning to maintain accuracy with minimal human effort.³

Selective classification – also called classification with rejection, learning with rejection, or misclassification detection – allows a model to abstain when its prediction is unreliable [8, 9, 11, 20, 21, 29, 47, 49]. Malware frameworks such as Transcendent [5], DroidEvolver [43], and CP-Reject [26] embed this mechanism. The objective is to minimize the *selective risk*, expected misclassification cost, while maximizing *coverage*, the share of accepted predictions [12]. Practically, this is realized via a confidence estimator whose threshold acts as a “dial”: tightening it lowers the error rate at the expense of accepting fewer samples, and vice versa.

Building on the same principle, production security scanners already quarantine files whose risk exceeds a preset threshold, deferring their release until an analyst can vet them [14, 40]. Once a detector is deployed, however, ground-truth labels are unavailable, so headline metrics such as F1 cannot be recomputed; the model’s own confidence serves as the sole proxy for decision quality. By calibrating a fixed monthly rejection quota in a hold-out window, we transform the confidence score into an operational “risk dial” in the spirit of Chow’s optimal reject rule [8] and modern selective-classification theory [12]. This ensures that (i) end-users are shielded from the most doubtful predictions and (ii) scarce analyst effort is directed toward the samples most likely to be misclassified, satisfying both safety and annotation-budget constraints.

Continual learning (CL) incrementally adapts a model to a non-stationary data stream and is often termed incremental or lifelong learning [42]. Classical CL assumes labels are plentiful throughout training – a condition seldom met. Active continual learning (ACL) addresses this gap by using active learning to query only the most informative points [42]. The dominant query rule is uncertainty sampling: select inputs for which the model is most unsure, thereby sharpening the decision boundary. A standard baseline measures this uncertainty with the classifier’s posterior, treating samples with $p \approx 0.5$ (binary case) as lying in the “uncertainty region” where confidence is lowest. Existing active-learning studies for malware detection each introduce bespoke uncertainty scores. CADE flags samples whose distance to class centroids (normalized by median absolute deviation) exceeds a threshold [44]; HCC computes a pseudo-loss from contrastive pairings with training neighbors [7]. We formalize both criteria in §4.3.

Confidence-based selection relies on the premise that a model’s confidence scores must correlate with true predictive risk. In a well-calibrated system, samples given high OOD scores or large predictive uncertainty should coincide with misclassifications, signaling that the model recognizes when it ventures beyond its training distribution. **The reliability of selective classification and active learning therefore depends on calibrated confidence estimates.** When calibration degrades – an outcome especially likely under distribution shift [17] – two problems arise. Selective

³Conceptually, rejected samples in selective classification are natural candidates for continual learning.

classification may pass high-confidence errors while discarding easy cases, and active learning may waste limited annotation budget on uncertain yet uninformative samples, overlooking those the model truly finds difficult (Figure 1). AURORA addresses this gap by quantifying how effectively a classifier’s confidence or OOD score orders inputs by their actual error probability and by validating this alignment under simulated temporal drift and resource constraints.

3 AURORA

The decomposition work by Rabanser and Papernot [35] establishes that ranking error – the misalignment between confidence scores and true correctness – constitutes a distinct failure mode in selective classification that calibration alone cannot address. Since monotone calibration methods preserve the underlying score ordering, they reduce approximation error but leave ranking error intact. Moreover, their decomposition identifies distribution shift as one of the “dominant practical sources of looseness,” yet their evaluation primarily considers isolated shift events (single corruption levels, fixed OOD test sets) rather than the sustained, evolving drift encountered in operational malware detection. This gap motivates our evaluation framework, which explicitly measures both reliability, whether confidence correctly ranks errors, and temporal stability, whether this ranking, and the classifier’s overall behavior, remains consistent as the data distribution evolves over time. These properties frame our two research questions for assessing SOTA Android malware classifiers under realistic deployment conditions:

- **RQ1:** How reliable are the OOD scores of SOTA Android malware classifiers under distribution shift?
- **RQ2:** How temporally stable are SOTA Android malware classifiers with respect to baseline performance and under selective classification conditions?

We first benchmark reliability, that is the degree to which a model’s confidence function correctly orders predictions by their true probability of error. Operationally, a reliable confidence function assigns higher uncertainty to incorrect predictions than to correct ones, enabling effective selective classification and sample prioritization. We quantify this property using the Risk–Coverage (RC) curve and its scalar summary, AURC, which directly measure the quality of this confidence-induced ranking (§3.2.2). To assess whether reliable ranking translates into practical benefit, we additionally report the Benefit Frequency (BF*), capturing how often abstention improves F1 relative to a no-rejection baseline (§3.3.3). We next probe temporal stability, that is the robustness of a model’s predictive performance and rejection behavior over time under distribution shift. Stability reflects whether a classifier behaves predictably as the data stream evolves – both in the absence of abstention and when operating as a selective classifier. Without abstention, we characterize performance stability using the standard deviation $\sigma[F1]$, measuring month-to-month volatility, and the Mann–Kendall statistic τ , detecting monotonic performance trends (§3.3.1, §3.3.2). Under selective classification, we assess operational stability via rejection bias and variability (ΔRej , $\sigma[\text{Rej}]^*$), which indicate whether the confidence-based quota mechanism reliably tracks its target under drift (§3.3.4). Section 3.1 details the monthly selective classification protocol underlying all experiments.

Non-Stationary Evaluation Setting. Our evaluation framework is explicitly designed for non-stationary malware classification, where concept drift continuously shifts the data distribution [23, 33]. Standard machine learning evaluation assumptions – such as i.i.d. samples and stable decision boundaries – do not hold in this setting. As established by prior work [32], temporal evaluation with strict train-test temporal ordering is essential for realistic assessment of malware classifiers. Throughout, we denote by \mathcal{D}_0 the fully-labeled bootstrap set (first 12 months of data), by M_i the batch of samples arriving in calendar month i of the test stream ($i = 1, \dots, N$), and by $B_{M_i} \in \{50, 100, 200, 400\}$ the monthly annotation budget selected via the model’s confidence function κ . The rejection-budget of online selective classification is denoted as ρ . These symbols underpin the temporal active continual learning protocol described in detail in Section 4.2.

Threat Model. We inherit the threat model from selective classification literature, where the primary challenge is natural distribution shift. In Android malware detection, this arises from malware evolution, benign app updates, and fragile feature spaces that violate i.i.d. assumptions. Under stationary distributions, existing methods achieve strong performance; our evaluation examines whether selective methods maintain their core operational properties – reliable confidence ranking, consistent rejection behavior, and temporal stability – under natural distribution drift. We assume realistic deployment constraints: limited annotation budgets and no ground-truth labels post-deployment, making confidence functions the sole signal for operational decisions.

3.1 Online Assessment via Selective Classification

SOTA approaches escalate the most uncertain apps (typically the top $\rho = B$ by an uncertainty proxy) to analysts [7, 44]. Instead of first issuing a prediction *and then* flagging those cases for review, we abstain *immediately* on that same fraction. Production scanners already quarantine suspicious files *before* exposing any verdict [14, 40]. Adopting this safety-first stance, we reject highest-uncertainty apps upfront – aligning with Chow’s risk-optimal reject rule [8] that minimizes expected cost when ground-truth is unavailable.

Let ρ be the desired rejection quota (e.g. $\rho = 400$ apps/month) and let S_{M_i} denote the stored uncertainty scores for the i -th calendar month M_i in the temporally ordered test stream $\mathcal{D}_{\text{test}} = \{M_1, \dots, M_N\}$. At the beginning of every month, we fit a threshold on *unlabeled* scores from a rolling window of preceding months and then freeze it for the duration of M_i :

- for single-valued OOD scores we learn a *single cut-off* c_i , above which samples are rejected;
- for soft-max probabilities in binary classification we learn a *rejection band* $[\ell_i, u_i]$ centered on maximal uncertainty ($\ell_i \leq S \leq u_i$ are rejected).

Thresholds are derived by selecting the $[\rho]$ -th most uncertain score in the calibration pool (cf. Algorithm 1 in Appendix C). The procedure adapts to slow drift by appending each month’s scores to the calibration pool. Two deployment-level diagnostics are collected: *stability* – how tightly the realized rejection rate follows ρ under drift – and *benefit* – the performance improvement from

discarding uncertain inputs. Only when the test-time score distribution matches the calibration window will the realized rate equal ρ (cf. Figure 3). We denote metrics computed under the post-hoc simulated SC protocol with * in Table 1.

Post-hoc simulated SC protocol
Monthly loop for M_i ($i = 1, \dots, N$):
P1. Calibrate: on the <i>unlabeled</i> score pool from prior months, estimate a cut-off c_i (or band $[\ell_i, u_i]$ for softmax) rejecting a fraction of inputs <i>on average</i> .
P2. Abstain: apply the threshold(s) to all samples in M_i ; scores above c_i (or inside $[\ell_i, u_i]$) are diverted to human analysts.
P3. Auto-classify: issue model predictions for the remaining in-coverage samples and compute coverage-adjusted performance, e.g., F1 score.
P4. Append: merge all scores from M_i with the calibration pool in preparation for M_{i+1} .

3.2 Assessing Reliability

3.2.1 Discrimination Ability (AUROC). The Area Under the Receiver Operating Characteristic curve (AUROC) measures a classifier’s ability to discriminate between malware and benign samples, independent of any decision threshold. AUROC quantifies the probability that a randomly chosen malware sample receives a higher predicted probability than a randomly chosen benign sample. Values range from 0.5 (random guessing) to 1.0 (perfect discrimination). Unlike F1, AUROC is threshold-independent and class-imbalance robust, making it a complementary baseline metric. However, AUROC alone does not capture confidence calibration – a model may achieve high AUROC while assigning poorly ranked confidence scores. We therefore report AUROC alongside AURC: the former assesses raw discrimination, while the latter evaluates whether confidence scores correctly order predictions by their probability of being correct.

3.2.2 Risk–Coverage Curves. High test accuracy is meaningless if the confidence function κ cannot rank predictions: selective classification and active learning both depend on reliable uncertainty estimates [29]. We therefore adopt the Risk–Coverage (RC) curve and its scalar summary, the Area Under the RC Curve (AURC) [13], to verify whether a classifier “*knows what it does not know*”. The RC curve concisely depicts a model’s uncertainty profile [10].

For the retained set $X_h \subseteq X$,

$$\text{coverage} = \frac{|X_h|}{|X|}, \quad \text{risk} = L(\hat{Y}_h), \quad (1)$$

and, for binary tasks,

$$\text{err} = \frac{1}{N} \sum_{n=1}^N |\hat{y}_n - y_n|, \quad (2)$$

where $\hat{y}, y \in \{0, 1\}$. As lower-confidence samples are admitted, coverage rises and a well-behaved RC curve stays flat before increasing smoothly (Figure 2); AURC integrates this behavior into a single risk score.

Link to Model Calibration. Confidence quality can also be judged by calibration. Expected Calibration Error (ECE) bins predictions by confidence and compares mean confidence with empirical accuracy [30]. **Selective prediction and confidence calibration are not inherently correlated** [10]: identical scores for all samples achieve perfect calibration (ECE= 0) but enable no ranking, whereas perfectly ordered scores {0.9, 1.0} may yield poor calibration (ECE= 0.9). Consequently, we prioritize ranking fidelity as captured by RC/AURC. Since any confidence score can be converted into a selective classifier [12], the RC framework offers a model-agnostic test. This concept has also gained attention in the security domain; for instance, Figure 1 in [5] illustrates several approaches to constructing alternative confidence functions from an array of different models.

3.2.3 F1–Risk Coverage (AURC[F1]*). Standard AURC summarizes a model’s *risk–coverage* trade-off by using error rate (1–accuracy) as the risk and sweeping a coverage threshold over the test set. In deployment, however, we do not have access to the full, time-spanning pool of confidence scores needed for this offline sweep. We therefore define AURC[F1]* as an *operational* risk–coverage metric computed under our post-hoc selective classification protocol (Protocol 3.1). Concretely, for each target coverage level c (equivalently, target rejection rate $1 - c$), we *calibrate* a rejection threshold using only the *unlabeled* rolling window of prior months, choosing the cut-off so that the protocol rejects approximately a fraction $(1 - c)$ of inputs *on average*. We then *freeze* this threshold for the current month, abstain on the most uncertain apps, and evaluate F1 on the retained (auto-classified) samples.

Formally, let $\hat{F}_1(c)$ denote the F1 score achieved on the non-rejected samples when the monthly threshold is calibrated to target coverage c . We define the corresponding risk as

$$R_{F1}(c) = 1 - \hat{F}_1(c) \quad (3)$$

and compute AURC[F1] as the area under $R_{F1}(c)$ integrated over $c \in [0.05, 1.0]$. This range spans near-complete rejection (5% coverage) up to full acceptance, capturing performance across 95% of the rejection spectrum. Lower AURC[F1] indicates that selective classification preserves high F1 as coverage decreases, under the same rolling, unlabeled calibration constraints faced at deployment. In this sense, AURC[F1]* is the online counterpart of offline AURC: instead of sweeping thresholds with global knowledge of scores, we sweep *target coverages* and realize them via the post-hoc rejection protocol.

Why AURC[F1]* complements AURC. AURC based on error rate treats all mistakes uniformly, but in malware detection the costs of false negatives (missed malware) are typically higher than false positives, since a single missed threat can trigger compromise. F1 (the harmonic mean of precision and recall) is sensitive to both error type and class imbalance, and therefore better reflects whether abstention preserves balanced detection quality rather than only improving overall accuracy. AURC[F1]* can thus distinguish methods that rank “easy vs. hard” samples well in an accuracy sense, from methods that do so while maintaining a healthy precision–recall trade-off. For example, a confidence function may achieve low AURC (good error ranking) yet yield high AURC[F1]* if abstention

disproportionately removes one class or degrades either precision or recall among the retained samples.

3.3 Assessing Stability

3.3.1 Performance Volatility ($\sigma[F1]$). The standard deviation $\sigma[F1]$ directly measures month-to-month volatility in classification performance. While CV normalizes by the mean, $\sigma[F1]$ provides the absolute scale of fluctuation, which operators may prefer when comparing models with similar baseline performance. Lower values indicate more predictable behavior across evaluation periods. Combined with τ , volatility admits a richer interpretation: low $\sigma[F1]$ with $\tau \approx 0$ signals operational stability, whereas high $\sigma[F1]$ with $\tau \approx 0$ indicates chaotic response to episodic drift – both metrics together distinguish robust adaptation from fragile oscillation.

3.3.2 Mann-Kendall Trend Statistic (τ). The Mann-Kendall statistic τ [27] is a non-parametric test for monotonic trends in time-series data. Applied to monthly F1 scores, $\tau > 0$ indicates improving performance over time, $\tau < 0$ signals systematic degradation, and $\tau \approx 0$ suggests no consistent directional trend. Unlike parametric alternatives, Mann-Kendall makes no distributional assumptions, making it suitable for the non-stationary malware setting.

Interpretation with $\sigma[F1]$. The τ statistic is most informative when non-zero: $\tau < 0$ provides early warning of model decay that $\sigma[F1]$ alone might miss – a method could exhibit moderate volatility while steadily degrading. However, τ is magnitude-blind (it counts directional changes, not their size) and cycle-blind (it cannot detect periodic patterns). Consequently, $\tau \approx 0$ is ambiguous without context: a robust method maintaining steady performance and a fragile method oscillating wildly with drift episodes can both yield $\tau \approx 0$. The distinction emerges from $\sigma[F1]$: $\tau \approx 0$ with low $\sigma[F1]$ indicates genuine stability, whereas $\tau \approx 0$ with high $\sigma[F1]$ reveals episodic sensitivity to drift.

3.3.3 Benefit Frequency (BF*). The Benefit Frequency (BF*) quantifies the proportion of evaluation periods in which selective classification improves F1 over the no-rejection baseline:

$$BF^* = \frac{1}{N} \sum_{i=1}^N \mathbf{1}[F1_i^* > F1_i],$$

where $F1_i^*$ denotes F1 after abstention in month i and $F1_i$ is the baseline. A BF^* of 50% indicates break-even; values above 50% suggest that abstention consistently helps, while values below reveal that the confidence function frequently misdirects rejections – removing correct predictions rather than errors. This metric complements AURC: while AURC measures ranking quality on a single distribution, BF^* captures whether that ranking translates to tangible benefit under the adaptive thresholding of operational selective classification across shifting distributions.

3.3.4 Rejection Stability. Rejection stability quantifies how consistently a selective classification mechanism tracks its target quota ρ under drift, capturing both systematic bias and temporal variability in realized rejections.

• **Rejection Bias (ΔRej^*).** For each month i , let ρ_i^* denote the actual number of rejections. The mean deviation from the target

quota:

$$\Delta Rej = \frac{1}{N} \sum_{i=1}^N (\rho_i^* - \rho).$$

$\Delta Rej > 0$ indicates systematic over-rejection (more analyst workload than planned), while $\Delta Rej < 0$ signals under-rejection (potential missed detections). Ideally, $\Delta Rej \approx 0$.

• **Rejection Variability ($\sigma[Rej]^*$).** The standard deviation of realized rejections:

$$\sigma[Rej]^* = \text{std}(\rho_1^*, \dots, \rho_N^*).$$

High $\sigma[Rej]^*$ reveals erratic behavior – some months vastly exceed the quota while others fall short – complicating resource planning. A well-behaved confidence function exhibits low $\sigma[Rej]^*$ alongside $\Delta Rej \approx 0$, indicating that the rejection mechanism tracks its target despite distributional drift [5].

4 Experimental Setup

We present the reference frameworks under evaluation (§4.1) and their training set-up (§4.2) followed by a description of the datasets adopted (§4.4).

4.1 Reference Frameworks

We evaluate four open-source Android malware classifiers that mark the field's shift from linear decision boundaries to contrastive representation learning. *Drebin* combines lightweight static analysis with a linear SVM on high-dimensional binary features [2]. *DeepDrebin* replaces the SVM with a fully connected network first introduced for adversarial robustness and later adopted for malware detection [16, 46]. *CADE* learns a contrastive embedding that tightens within-class clusters and sharpens out-of-distribution (OOD) separation. We use the enhanced variant from [7], which swaps the original SVM for a neural classifier and feeds it the learned embeddings. Building on this approach, *HCC* extends the contrastive learning idea with a hierarchical loss function that imposes family-level similarity constraints [7]. We exclude *DroidEvolver* [43] due to its self-poisoning risk from pseudo-label retraining [24]. *Transcendent* [5] is omitted as a purely selective-classification method that does not use drift signals for downstream adaptation; while it inspired our focus on rejected-sample performance, we defer its evaluation to future work. We report hyperparameter settings in Appendix D and repeat each experiment with five random seeds for statistical reliability.

4.2 Active Learning Setup

To benchmark our methods under realistic data streams, we adopt the *temporal active learning* protocol outlined below. The data corresponding to the first twelve calendar months of every dataset constitute a fully-labeled bootstrap set \mathcal{D}_0 , after which the stream is processed month-by-month. Let M_i denote the set of samples arriving in month i ($i = 1, \dots, N$). In each cycle, the current model is evaluated on the unseen portion of M_i , queries the $B_{M_i} \in \{50, 100, 200, 400\}$ most uncertain instances according to its confidence function κ , receives human annotations, and is then updated before advancing to M_{i+1} . The budget levels $B_{M_i} \in \{50, 100, 200, 400\}$ align with the de facto standard from prior Android malware active learning work,

including Chen et al. [7], and followed by subsequent frameworks like LAMD [34] and CITADEL [18].

Active Learning on Temporal Datasets

Initialisation. First 12 months → fully-labeled training set \mathcal{D}_0 . Pretrained model on \mathcal{D}_0 .

Monthly loop for M_i ($i = 1, \dots, N$):

- P1.** *Evaluate* on the unseen samples M_i .
- P2.** *Query* the B_{M_i} most-uncertain instances via κ ($B_{M_i} \in \{50, 100, 200, 400\}$ [7, 44]).
- P3.** *Annotate* queried instances with human-provided labels.
- P4.** *Update* the model: append new labels to the training pool and retrain either *cold* (from scratch) or *warm* (incrementally) before moving to M_{i+1} .

The annotator supplies both binary and family labels, although only HCC requires the latter. Following [7], HCC is warm-started, CADE is evaluated in both cold- and warm-start settings, and DeepDrebin and Drebin are retrained from scratch.

4.2.1 Initial Dataset Configurations. In addition to training on the full initial dataset \mathcal{D}_0 , we evaluate configurations where \mathcal{D}_0 is subsampled to $B_0 = 4800$ samples using stratified random draws. This budget-proportional subsampling explores whether the large volume of historical data in \mathcal{D}_0 may impede adaptation to drift, as the gradient signal from fresh monthly samples (B_{M_i}) can be overwhelmed by abundant but potentially outdated patterns. Our experiments show that subsampling often improves or maintains performance while reducing computational cost. The full investigation, including methodology, results, and analysis, is presented in Appendix E. This observation aligns with recent findings on data pruning [38].

4.3 Confidence Functions for Uncertainty and OOD Detection

We extract confidence scores from each model to quantify prediction uncertainty and identify out-of-distribution (OOD) samples. These scores, denoted $\kappa(x)$, either represent native confidence measures (e.g., softmax probabilities or Drebin margin distances) or model-specific OOD detection scores. Below, we outline the core mechanisms across different model types.

4.3.1 Softmax-Based Confidence. For neural classifiers with a softmax output layer, we use the *Maximum Softmax Probability* (MSP) as a native confidence score. Given an input x and a neural model with logits $f(x) \in \mathbb{R}^K$, the softmax probability for class k is:

$$p_k(x) = \frac{\exp(f_k(x))}{\sum_{j=1}^K \exp(f_j(x))}$$

The model's confidence is $\kappa(x) = \max_k p_k(x)$. To derive an uncertainty score, we normalize its deviation from the binary decision boundary (0.5):

$$U(x) = 1 - \frac{|\kappa(x) - 0.5|}{0.5}$$

This formulation reflects confidence as proximity to maximal uncertainty and aligns with nonconformity scores in conformal prediction frameworks [5, 23, 37].

4.3.2 Drebin Margin-Based Confidence. For Support Vector Classifiers (SVC), we use the (signed) distance from a sample x to the separating hyperplane $f(x) = \mathbf{w}^\top x + b$:

$$\kappa(x) = \frac{f(x)}{\|\mathbf{w}\|}$$

Larger distances (in magnitude) indicate higher confidence in the predicted label.

4.3.3 CADE OOD Score. CADE employs contrastive learning and computes an OOD score based on deviation from class centroids in the latent space. For a test sample x , its score relative to class i is:

$$A_i(x) = \frac{|d_i(x) - \tilde{d}_i|}{\text{MAD}_i}$$

where $d_i(x)$ is the distance to the class centroid c_i , \tilde{d}_i is the median intra-class distance, and MAD_i is the scaled median absolute deviation. The final score is $\kappa(x) = \min_i A_i(x)$, and samples with $\kappa(x) > \tau$ ($= 3.5$) are classified as OOD.

4.3.4 HCC Pseudo-Loss Score. HCC defines uncertainty using a pseudo-loss in a contrastive setting. Each test sample x embedding is compared with its nearest training neighbors. A binary label is then assigned to x , and the pseudo-loss is:

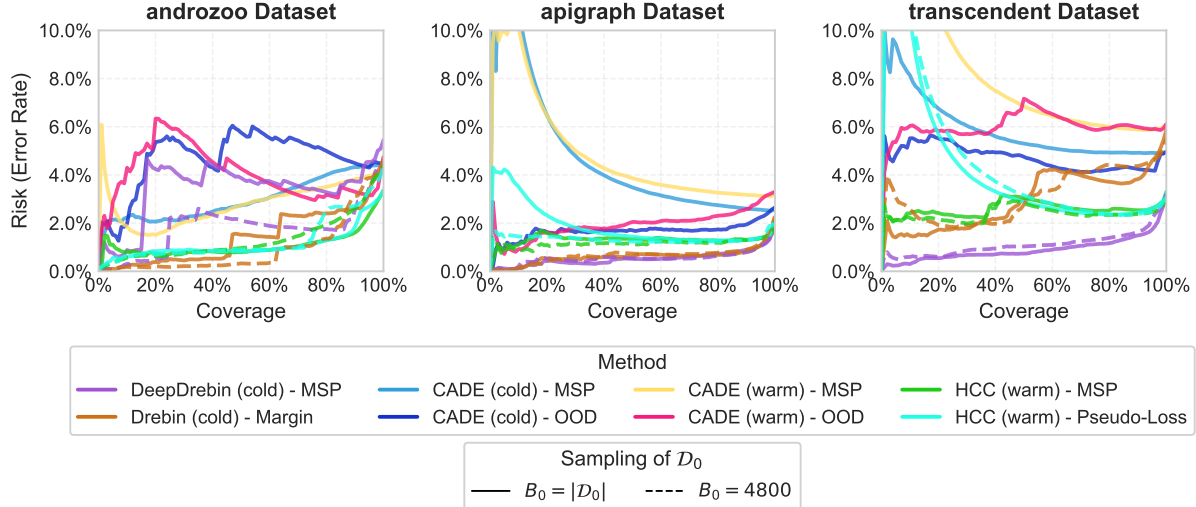
$$\kappa(x) = \hat{L}_{\text{hc}}(x) + \lambda \hat{L}_{\text{ce}}(x)$$

where \hat{L}_{hc} is a contrastive hinge loss and \hat{L}_{ce} is a binary cross-entropy loss. Higher pseudo-loss indicates greater uncertainty or potential OOD status.

4.4 Datasets

The experiments are conducted on three datasets: APIGraph and Androzoo from [7] and Transcendent from [5]. We selected these datasets as they are used in SOTA research, are well-established in the Android malware detection domain, and contain large sample collections with timestamps to simulate natural temporal drift. For the APIGraph dataset, the authors from [7] collected Android apps using hashes from APIGraph [46], but extracted Drebin features rather than using the feature space originally proposed in that work. When we reference the APIGraph dataset, we are specifically referring to the dataset introduced by Chen et al. [7]. The APIGraph dataset contains Android apps from 2012-2018 with a 9:1 malware-to-goodware ratio, while Androzoo spans 2019-2021 with the same ratio. Transcendent includes apps from 2014-2018, also maintaining the 9:1 ratio, as recommended by Pendlebury et al. [33]. Across all datasets, we treat the first year as an initial training buffer \mathcal{D}_0 , where we assume full label availability. As common practice [7], we use a monthly evaluation- and retraining cycle which we denote as $\mathcal{D}_{\text{test}}$. As in [7], we use the first 6 months from $\mathcal{D}_{\text{test}}$ to select the best hyperparameters for each method. The reported results exclude the initial 6-month period of $\mathcal{D}_{\text{test}}$ to avoid data snooping [1].

Figure 2: Risk-Coverage Plots for selected datasets and for a label-budget $B_{M_i} = 50$. The ideal curve has minimal error across the coverage-spectrum and a higher coverage or *acceptable uncertainty* correlates with a higher error. The dashed line refers to models trained with a sub-sampled initial data-set \mathcal{D}_0 (with $B_0 = 4800$).



4.4.1 Computational Requirements. We observe a substantial disparity in computational requirements across methods. On the Transcendent dataset (48 test months, $B_{M_i} = 200$), Drebin and DeepDrebin require approximately 2 and 20 minutes total respectively, while contrastive methods impose significantly higher costs: HCC (warm) 8.8 hours, CADE (warm) 15.9 hours, and CADE (cold) 28.8 hours on H100 GPU – over 800× longer than Drebin. Across five seeds per configuration, the full CADE/HCC experimental suite consumed approximately 2,500 GPU-hours. Regardless of whether we use MSP or Pseudo-Loss with HCC, or MSP and deviation from class centroids with CADE, the underlying model must be trained according to the respective CADE and HCC regimes. Both methods position their OOD scores as improved mechanisms for separating malware from goodware. However, this promised advantage does not consistently translate to empirical gains in realistic settings, where simpler baselines remain competitive.

5 Results

We apply AURORA to evaluate the reference frameworks and their associated confidence functions across three datasets under various training configurations ($B_{M_i} \in \{50, 100, 200, 400\}$) [7, 18, 34] and B_0 . Table 1 categorizes our evaluation metrics into three pillars:

- (1) Baseline performance: F1, FNR, and AUROC
- (2) Reliability of confidence functions: AURC, AURC[F1]*
- (3) Stability under temporal drift: $\sigma[F1]$, τ , BF^* , ΔRej^* , $\sigma[Rej]^*$

Figure 2 reveals the alignment between model confidence and prediction errors through risk-coverage curves (RQ1), and Figure 3 traces month-by-month evolution, exposing stability patterns under both standard and selective classification regimes (RQ2).

This multi-dimensional view exposes a central tension: *methods that excel on headline metrics often fail on operational criteria*

that matter for deployment. We structure our analysis around the research questions, with each subsection revealing instances of Goodhart’s Law – where optimizing for one measure conceals deficiencies exposed by another.⁴

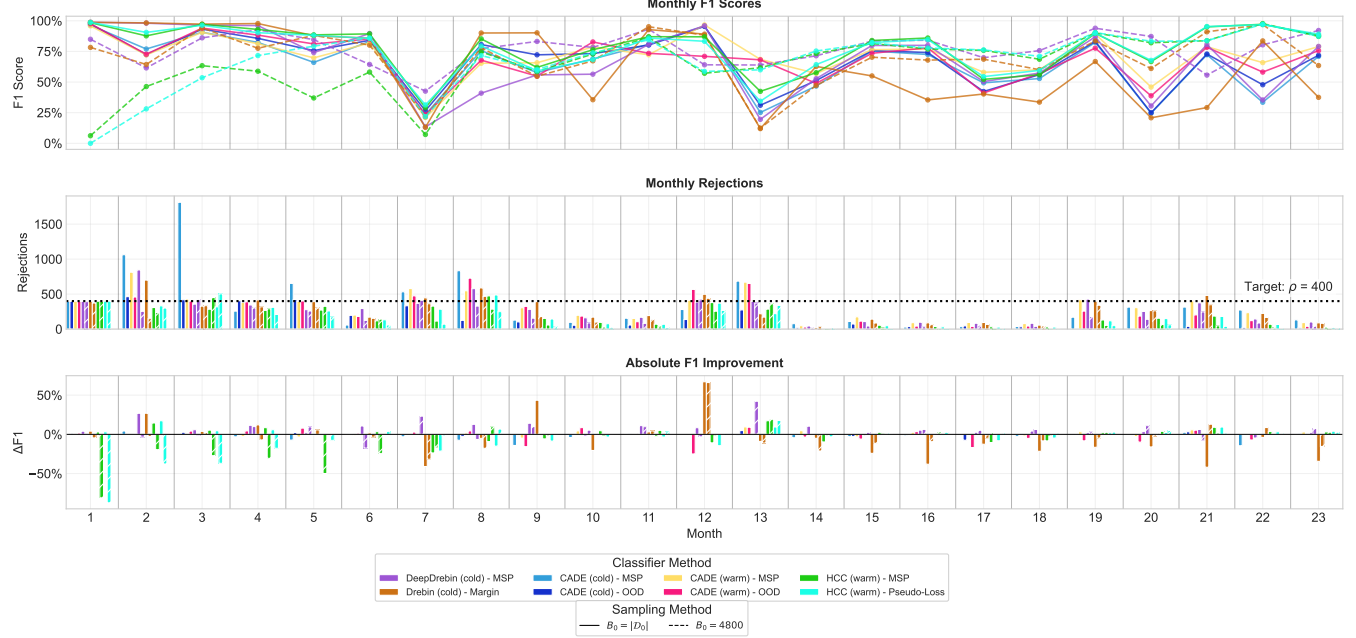
5.1 Answering RQ1: Does Confidence Quality Match Performance?

Table Interpretation. The table separates **Baseline** metrics from **Reliability** metrics (green background). To understand why this distinction matters, consider CADE-OOD and DeepDrebin Full on APIGraph at $B_{M_i} = 400$. Both achieve similar baseline F1 scores (89% vs 93%), suggesting comparable detection capability. But the reliability metrics paint a different picture. **AURC** measures confidence calibration – how well the model ranks its errors, with lower values indicating better calibration. CADE’s AURC=1.9 versus DeepDrebin’s AURC=0.3 reveals a 6× gap in confidence calibration: when selective classification is enabled, CADE’s high-confidence predictions are frequently wrong even at low coverage (Figure 2), while DeepDrebin maintains near-zero risk. **AURC[F1]*** uses F1-based risk (1 - F1) to reveal whether rejection maintains balanced precision-recall performance as coverage decreases (lower is better). CADE’s 32.0 versus DeepDrebin’s 4.8 means CADE disproportionately rejects one class – potentially abstaining on the very malware samples that matter most.

Headline Metrics Create False Confidence. Examining baseline F1 in Table 1, HCC achieves the highest scores on AndroZoo (85% at $B_{M_i} = 400$) and competitive results elsewhere. CADE variants lag

⁴We exclude FPR as all methods achieve very low rates, making it uninformative. We prioritize FNR because missed malware carries higher operational risks than false alarms [6, 22]. We omit the Area Under Time (AUT) [32] metric as it essentially duplicates average metrics. We also omit AURC under simulated SC since fixed rejection thresholds represent segments of the full RC curve without additional insights.

Figure 3: Temporal results for models trained on the *androzoo* dataset with $B_{M_i} = 50$ and for $\rho = 400$. The top-row presents the F1 score after simulated selective classification. The middle depicts the actual rejections on a monthly basis and in the bottom row is the improvement in F1 after rejection vs. the baseline of no rejections as $\Delta F1$. The latter highlights that rejections does not always lead to improvements with respect to F1 scores for some methods.



behind, particularly on Transcendent where F1 drops to 74–77%. DeepDrebin with subsampling ($B_0 = 4800$) matches or exceeds HCC on AndroZoo while maintaining the best APIGraph performance (93% F1). These headline numbers suggest clear winners – but they obscure the reliability of the underlying confidence functions.

Tensions. The AURC results expose a critical disconnect with F1. On AndroZoo, DeepDrebin Full achieves baseline F1 of only 54–71% yet maintains competitive AURC at higher budgets, while CADE exhibits acceptable F1 but the worst AURC. On APIGraph, the gap is stark: DeepDrebin achieves AURC as low as 0.3 at $B_{M_i} = 400$, while CADE-OOD ranges from 1.6 to 3.3 – a 5–10× difference despite only 4–6% F1 difference. **High F1 does not imply calibrated uncertainty.** However, even well-calibrated models exhibit a second tension. We designed AURC[F1]* to detect class-imbalanced rejection behavior masked by good aggregate error ranking. On AndroZoo at $B_{M_i} = 200$, HCC-MSP achieves AURC=1.0 but AURC[F1]*=55.1, while DeepDrebin with $B_0 = 4800$ achieves AURC[F1]*=6.9 – nearly 8× better. HCC’s confidence function ranks total errors well but disproportionately rejects one class. On Transcendent, CADE-MSP exhibits AURC[F1]*=40.4 at $B_{M_i} = 200$, the worst score, demonstrating that its rejection strategy undermines balanced detection despite reasonable total error ranking.

RC Curve Analysis (Figure 2). The Risk-Coverage curves at $B_{M_i} = 50$ decompose these AURC findings. Three patterns emerge: (1) DeepDrebin maintains near-zero risk across most coverage levels on APIGraph and Transcendent, with curves staying flat until high

coverage – indicating well-calibrated confidence. (2) CADE exhibits severe miscalibration at low coverage, where reliable uncertainty quantification matters most. On Transcendent, CADE-MSP reaches ~40% risk even at 20% coverage, meaning high-confidence predictions are frequently wrong. (3) HCC shows intermediate behavior: better than CADE but with steeper risk increases at moderate coverage on AndroZoo.

RQ1 Takeaways: (1) Headline F1 provides no guarantee of confidence calibration – methods with similar F1 can differ by 10× in AURC. (2) Low AURC (good error ranking) does not imply balanced class behavior under rejection; AURC[F1]* exposes this gap. (3) CADE’s distance-based OOD scoring fails precisely at low-coverage operating points where abstention matters most. (4) DeepDrebin with subsampling achieves the best overall reliability profile with only binary labels and modest compute. (5) Selective classification can *hurt* performance for poorly calibrated methods – Drebin’s F1 degrades with increased rejection.

5.2 Answering RQ2: Does Performance Persist Over Time?

Table Interpretation. The **Stability** metrics (blue background) expose temporal robustness across evaluation periods. Consider

Table 1: Comprehensive evaluation across monthly budgets B_{Mi} . Baseline: F1=detection rate; FNR=false negative rate; AUROC=discrimination ability. Reliability (green): AUROC=uncertainty calibration (error-based risk); AUROC[F1]^{*}=area under F1-risk curve (risk = 1-F1) over coverage $c \in [0.05, 1.0]$. Stability (blue): $\sigma[F1]$ =F1 volatility; τ =Mann-Kendall trend (>0 =improving); BF*=Benefit Fraction (% of months where SC improves F1); ΔRej^* =rejection bias (closest to 0=best); $\sigma[Rej]^*$ =rejection std. B_0 : Full=full first year, 4800=subsampled. Metric arrows (\uparrow/\downarrow) indicate whether higher or lower values are better. Pareto (P): Pareto optimality within each B_{Mi} using dataset-averaged F1, $\sigma[F1]$, AUROC, and τ ; \star =non-dominated, \circ =dominated. Bold=best, red=worst per metric-dataset within each B_{Mi} .

B_M	B_0	Method	Baseline						Reliability						Stability																		
			P	F1 (%) \uparrow			FNR (%) \downarrow			AUROC \uparrow			AUROC \downarrow			AUROC[F1] \downarrow			$\sigma[F1]\downarrow$			$\tau\uparrow$			BF \uparrow			ΔRej^*			$\sigma[Rej]^*\downarrow$		
				AZ	AP	TR	AZ	AP	TR	AZ	AP	TR	AZ	AP	TR	AZ	AP	TR	AZ	AP	TR	AZ	AP	TR	AZ	AP	TR	AZ	AP	TR			
$B_M=50$	B_0	Full DeepDrebin	o	54	90	83	58	15	19	74.0	96.8	95.4	5.5	0.5	1.4	34.3	7.2	6.3	23.3	4.4	8.7	0.25	0.41	-0.03	78	100	100	-17	+5	+12	77	33	37
		Full HCC-PL	o	75	89	83	34	16	19	63.1	89.1	85.0	1.3	1.7	4.7	60.3	7.8	12.4	17.8	4.1	8.2	0.09	0.17	-0.07	100	100	90	-28	+19	-3	31	45	68
		Full HCC-MSP	\star	75	89	83	34	16	19	94.0	93.8	92.3	1.3	1.3	3.2	61.0	8.6	16.9	17.8	4.1	8.2	0.09	0.17	-0.07	99	100	91	-26	+19	+1	34	46	71
		Full Drebin	o	63	88	71	50	18	39	73.4	90.7	89.5	1.7	0.6	1.7	72.0	6.7	22.4	21.7	4.7	13.9	0.10	0.25	-0.11	69	97	89	-36	-9	-14	14	29	25
		Full CADE-OOD	o	63	86	68	48	17	40	48.5	89.7	79.0	5.2	2.0	5.0	33.9	39.6	36.7	20.8	4.4	13.6	-0.16	0.08	-0.16	50	0	4	-50	-50	-40	0	0	11
		Full CADE-MSP	o	63	86	69	48	17	40	78.9	91.3	80.4	4.4	4.2	6.4	32.9	8.8	26.9	20.8	4.4	13.7	-0.16	0.08	-0.14	27	96	1	+47	+2	+514	140	36	572
$B_M=100$	B_0	4800 DeepDrebin	\star	71	90	81	40	15	27	91.4	96.7	91.7	1.6	0.6	1.9	18.2	6.3	15.5	19.5	4.3	8.7	0.15	0.37	0.17	81	99	100	-40	-11	-12	8	28	27
		4800 HCC-PL	o	72	89	83	39	16	20	51.4	88.6	85.8	1.1	1.3	4.2	38.9	9.0	14.6	16.5	4.5	7.9	0.56	0.28	-0.02	43	100	79	-24	-27	+53	52	19	74
		4800 HCC-MSP	\star	72	89	83	39	16	20	94.4	93.8	93.4	1.1	1.1	2.5	42.8	9.2	15.7	16.5	4.5	7.9	0.56	0.28	-0.02	60	100	92	-39	-22	+11	20	21	32
		4800 Drebin	\star	69	88	74	42	17	36	76.1	90.9	88.9	1.1	0.6	1.8	67.8	7.2	24.4	20.5	4.6	11.6	0.25	0.24	-0.04	33	100	97	-34	-24	-23	20	24	18
		Full DeepDrebin	o	59	91	85	54	13	15	72.8	97.1	96.1	6.0	0.6	1.1	32.3	6.9	4.1	22.9	3.9	8.5	0.16	0.41	0.05	83	100	100	-60	+4	+42	30	62	77
		Full HCC-PL	o	77	90	84	32	14	17	73.7	92.5	82.7	1.0	1.4	4.9	55.5	6.4	11.7	16.3	3.9	7.7	0.25	0.14	-0.14	99	100	100	-37	-21	-18	112	48	84
$B_M=200$	B_0	Full HCC-MSP	o	77	90	84	32	14	17	95.2	94.6	92.8	1.0	1.3	2.0	55.5	7.6	15.9	16.3	3.9	7.7	0.25	0.14	-0.14	100	100	100	-33	-9	-17	112	56	85
		Full Drebin	\star	68	88	78	43	17	29	75.4	91.3	90.6	1.2	0.6	1.4	63.8	6.8	17.7	21.5	4.4	11.3	0.18	0.17	-0.08	69	99	83	-43	+2	-28	44	85	57
		Full CADE-OOD	o	63	87	71	48	16	39	55.2	91.1	81.5	5.8	1.8	4.6	37.1	38.4	33.1	21.1	3.9	12.9	-0.03	0.12	-0.18	50	50	29	-100	-100	-95	0	0	14
		Full CADE-MSP	o	63	87	71	48	16	38	75.9	91.7	81.9	5.2	3.6	4.6	32.6	7.0	41.3	21.1	3.9	13.1	-0.03	0.12	-0.22	28	100	0	+41	+95	+907	141	213	1069
		4800 DeepDrebin	\star	76	92	84	33	12	21	92.7	97.1	93.3	1.3	0.6	1.5	11.2	5.7	11.7	17.4	3.6	7.6	0.40	0.35	0.13	63	100	92	-70	-40	-23	50	39	45
		4800 HCC-PL	o	80	91	85	29	13	19	50.8	91.3	87.3	1.0	1.4	3.2	30.5	6.9	13.8	15.3	3.9	7.7	0.21	0.30	-0.01	100	100	70	-93	-60	+36	11	21	83
$B_M=400$	B_0	4800 HCC-MSP	\star	80	91	85	29	13	19	95.2	95.4	93.1	1.0	0.9	2.4	36.0	7.1	15.7	15.3	3.9	7.7	0.21	0.30	-0.01	98	100	94	-96	-49	+0	5	31	65
		Full Drebin	o	67	89	76	45	16	33	74.2	91.8	90.2	1.7	0.7	1.6	67.3	6.7	20.7	20.7	4.0	11.6	0.19	0.17	-0.14	74	100	100	-53	-45	-46	77	35	29
		Full DeepDrebin	o	60	92	87	54	12	12	74.3	97.4	96.8	5.5	0.4	0.9	27.4	6.0	3.6	19.8	3.6	7.6	0.18	0.38	0.12	65	100	98	-73	-39	+82	171	84	138
		Full HCC-PL	o	79	91	86	31	12	14	72.8	94.0	80.6	0.9	1.2	3.4	55.0	5.5	10.7	16.9	3.6	7.1	0.29	0.13	-0.05	67	100	45	-99	-67	+302	118	66	297
		Full HCC-MSP	o	79	91	86	31	12	14	95.4	95.6	94.2	1.0	0.9	2.2	55.1	6.4	13.5	16.9	3.6	7.1	0.29	0.13	-0.05	66	100	85	-99	-60	+106	115	75	171
		Full Drebin	o	69	89	81	42	16	25	76.3	91.6	90.9	1.1	0.7	1.2	54.3	6.1	13.8	20.9	4.0	10.9	0.18	0.16	-0.07	66	99	85	-123	-11	-37	61	121	107
$B_M=400$	B_0	Full CADE-OOD	o	68	89	74	44	14	35	62.7	92.7	80.9	4.3	1.6	4.2	32.4	3.3	30.0	17.4	3.7	11.8	0.10	0.08	-0.14	2	0	27	-193	-200	+68	10	1	238
		Full CADE-MSP	o	68	89	74	44	14	34	78.2	92.5	83.7	4.8	3.3	4.4	24.3	6.0	40.4	17.4	3.7	11.7	0.10	0.08	-0.18	21	100	0	-19	+968	+1478	199	1156	1769
		4800 DeepDrebin	\star	82	92	87	27	12	14	95.5	97.4	96.0	0.8	0.5	1.0	6.9	4.5	5.9	13.0	3.5	8.7	0.25	0.37	0.20	44	100	97	-144	-79	+14	96	71	114
		4800 HCC-PL	o	83	92	88	26	11	13	53.1	94.0	82.1	0.7	0.8	3.6	24.3	5.2	11.8	9.6	3.3	6.4	0.25	0.28	-0.05	86	100	60	-182	-153	+17	34	24	106
		4800 HCC-MSP	\star	83	92	88	26	11	13	96.6	96.3	94.6	0.7	0.7	2.4	28.6	5.5	12.7	9.6	3.3	6.4	0.25	0.28	-0.05	70	100	68	-188	-119	+20	29	46	101
		4800 Drebin	o	69	89	82	42	15	24	75.7	92.0	90.6	1.6	0.6	1.5	62.1	6.1	16.7	21.7	3.7	10.5	0.18	0.11	-0.01	93	100	98	-140	-51	-38	53	108	82
$B_M=500$	B_0	Full DeepDrebin	\star	71	93	90	41	11	8	83.0	97.7	97.6	3.5	0.3	0.7	14.3	4.8	2.8	20.0	3.3	7.2	0.46	0.38	0.02	98	100	100	-126	-77	+350	271	147	342
		Full HCC-PL	o	85	86	88	23	16	11	61.8	93.5	78.2	0.8	1.1	4.1	53.4	5.6	9.0	11.0	15.2	7.1	0.15	-0.15	-0.02	60	100	63	-211	-119	+384	216	600	389
		Full HCC-MSP	o	85	86	88	23	16	11	96.0	92.8	95.6	0.9	2.2	2.4	53.8	11.9	11.4	11.0	15.2	7.1	0.15	-0.15	-0.02	55	98	64	-146	-202	+343	328	101	379
		Full Drebin	o	71	89	83	39	16	20	77.1	91.6	90.0	0.9	0.6	1.6	4																	

low volatility ($\sigma[F1] \approx 3\text{--}5$) at budgets 50–200. However, an important collapse occurs at $B_{M_i} = 400$: HCC Full's $\sigma[F1]$ jumps from 3–4 to 15.2 (a $4\times$ increase), while DeepDrebin (both Full and with $B_0 = 4800$) maintains $\sigma[F1]=3.1\text{--}3.3$. HCC with $B_0 = 4800$ reports $\sigma[F1]=3.6$. This reversal demonstrates that stability rankings can flip dramatically with both monthly budget changes and initial training budget choices. On AndroZoo, the pattern differs: HCC maintains superior stability ($\sigma[F1]=11\text{--}17$) compared to DeepDrebin Full ($\sigma[F1]=19\text{--}23$), though DeepDrebin with $B_0 = 4800$ closes the gap ($\sigma[F1]=12\text{--}20$). CADE exhibits the worst stability on Transcendent, with $\sigma[F1]$ reaching 12–14 across budgets.

Tensions. The Mann-Kendall trend (τ) reveals distinct performance trajectories. DeepDrebin consistently improves on APIGraph ($\tau \approx 0.33\text{--}0.41$), while CADE variants degrade on Transcendent ($\tau = -0.22$ to -0.07). Together with performance variability ($\sigma[F1]$), we identify three distinct patterns: (1) Robust adaptation – stable performance with steady improvement (DeepDrebin on APIGraph); (2) Fragile oscillation – erratic performance without clear direction (CADE on AndroZoo at $B_{M_i} = 100$); (3) Systematic decay – moderate instability with declining performance (CADE on Transcendent). F1 does not imply good performance ($\sigma[F1]$) across all time-windows (months) of the evaluation-period or stable long-term performance (τ). The Benefit Fraction (BF^*) reveals when abstention actually helps. On APIGraph, DeepDrebin and HCC achieve $BF^*=100\%$ in most cases – meaning selective classification improves F1 every single month. By contrast, CADE-OOD manages only $BF^*=0\text{--}4\%$ in several configurations, essentially never benefiting from abstention. This failure is even more pronounced on Transcendent: at $B_{M_i} = 400$, CADE-MSP achieves $BF^*=1\%$, improving F1 in just 1 out of 48 months.

Rejection Consistency Under Drift. The ΔRej^* (bias) and $\sigma[Rej]^*$ (variability) metrics expose operational reliability of rejection mechanisms: (1) Drebin with $B_0 = 4800$ maintains moderate rejection consistency on AndroZoo with $\sigma[Rej]^*=20\text{--}135$ across budgets; (2) HCC Full exhibits systematic degradation across all datasets as budgets increase: on AndroZoo ($\sigma[Rej]^*$ from 31–34 to 216–328), APIGraph (45–46 to up to 600), and Transcendent (68–71 to 379–389), while subsampling ($B_0 = 4800$) maintains better consistency on AndroZoo and APIGraph but similarly degrades on Transcendent; (3) CADE-MSP exhibits *catastrophic* inconsistency: on Transcendent at $B_{M_i} = 400$, $\Delta Rej^*=+3375$ and $\sigma[Rej]^*=3347$ – meaning it overshoots the rejection quota by 3000+ samples on average with massive variability. At $B_{M_i} = 200$, $\Delta Rej^*=+1478$ and $\sigma[Rej]^*=1769$.

Temporal Evolution (Figure 3). The month-by-month analysis at $B_{M_i} = 50$, $\rho = 400$ reveals: (1) All methods experience F1 drops in Months 7 and 13, coinciding with drift events; (2) CADE variants frequently exceed rejection quotas by 3–5 \times , with Month 3 showing CADE-MSP rejecting >1500 samples against a target of 400; (3) The AF1 panel shows that rejection *decreases* F1 for some methods in certain months, confirming that $BF^*<100\%$ reflects real operational harm.

RQ2 Takeaways: (1) Stability rankings can reverse with budget changes – HCC's stability advantage at low budgets becomes a liability at $B_{M_i} = 400$ on APIGraph. (2) Selective classification is not universally beneficial; CADE achieves $BF^*<5\%$ in several configurations. (3) CADE's rejection mechanism is catastrophically unstable, overshooting quotas by 3000+ samples with important variability. (4) DeepDrebin with subsampling offers the best stability-performance trade-off across budgets. (5) The Mann-Kendall trend (τ) combined with $\sigma[F1]$ distinguishes robust adaptation from fragile oscillation and systematic decay.

5.3 The Pareto Perspective: No Universal Winner

Pareto Methodology. Multi-objective evaluation across all metrics simultaneously presents a methodological challenge: with 10+ metrics per dataset across 3 datasets, the *curse of dimensionality* renders Pareto analysis uninformative – in 30-dimensional objective space, nearly all methods become non-dominated simply by excelling on any single metric-dataset combination. To obtain meaningful discrimination, we aggregate metrics across datasets before computing dominance. Specifically, we average each of four pillar representatives – F1 (baseline performance), $\sigma[F1]$ (stability), AURC (reliability), and τ (trend) – across the three datasets, yielding a 4-dimensional Pareto analysis per budget B_{M_i} . A method is *dominated* (○) if another method achieves equal or better values on all four aggregated pillars and strictly better on at least one; otherwise it is *non-dominated* (★). This approach balances discrimination power (6–8 methods dominated per budget) against metric coverage (each pillar represents a distinct evaluation dimension).

Pareto Analysis Results. The tensions exposed above converge in a multi-objective reality: *no method dominates across all metrics and all conditions*. The Pareto column (P) in Table 1 reveals: (1) DeepDrebin with subsampling ($B_0 = 4800$) and HCC-MSP ($B_0 = 4800$) are consistently Pareto-optimal across all budgets, achieving the best F1-stability-trend-reliability trade-off; (2) DeepDrebin Full becomes Pareto-efficient only at $B_{M_i} = 400$, while Drebin Full is non-dominated only at $B_{M_i} = 100$; (3) CADE variants are dominated in all configurations – there always exists another method with better performance *and* better stability *and* better reliability; (4) HCC-MSP Full is non-dominated at $B_{M_i} = 50$ but becomes dominated at higher budgets due to stability degradation. A striking pattern emerges: subsampling the initial training data ($B_0 = 4800$) consistently outperforms using the full first year. Both DeepDrebin and HCC-MSP achieve Pareto-optimality with subsampling across all budgets, while their Full counterparts are often dominated. This suggests that strategic data curation during cold-start – selecting representative samples rather than using all available data – yields classifiers that are simultaneously more performant, more stable, and better calibrated. This analysis underscores the central message: deployment decisions cannot be made from F1 alone. The “best” method depends on operational priorities – workload predictability, trend direction, calibration quality – that headline metrics do not capture.

Takeaway: Our goal is not to crown a single winner, but rather to demonstrate that *evaluation methodology shapes method selection*. Just as TESSERACT [33] redirected the field toward temporal evaluation, AURORA highlights that operational deployment demands assessment along multiple dimensions beyond accuracy. The Pareto analysis reveals that introducing additional evaluation dimensions – confidence calibration, temporal stability, rejection consistency – fundamentally alters which methods appear “best.” A method that dominates under F1 may be dominated once AURC and σ_{Rej}^* are considered. This underscores our central argument: *measurement choices determine solution rankings. Designing methods that achieve both high stationary performance and reliable selective prediction under drift remains an open challenge – one that AURORA makes explicit and measurable.*

5.4 Practical Method Selection Guidelines

Our evaluation shows that apparent method superiority is highly contingent on the operational dimension being stressed. Methods that appear strong under static accuracy metrics often fail to preserve their advantage once calibration, workload stability, or temporal robustness are considered. High baseline F1 does not guarantee deployment robustness. Although HCC achieves the highest F1 on AndroZoo (85%) and Transcendent (88%) at large initial budgets ($B_0 = 4800$), this advantage is fragile: under tighter monthly budgets, performance on APIGraph degrades to the point that no meaningful separation remains. This sensitivity indicates that raw detection performance alone is insufficient for budget-constrained settings. Confidence reliability introduces a second axis of separation. DeepDrebin consistently produces substantially lower AURC values across all datasets – reaching 0.3 on APIGraph – indicating that its confidence estimates remain informative even under distribution shift. In contrast, methods with comparable F1 often exhibit confidence collapse, limiting the effectiveness of selective classification. Class-conditional rejection behavior further exposes hidden failure modes. On AndroZoo, DeepDrebin with subsampling reduces AURC[F1]* by 4–8× relative to HCC (6.9 vs. 55.1 at $B_{M_i} = 200$), whereas HCC’s abstention disproportionately suppresses one class. Such imbalance is invisible to aggregate rejection metrics but materially affects security outcomes. Operational predictability emerges as a hard constraint. CADE exhibits extreme variance in rejection behavior ($\sigma[\text{Rej}]^* > 1000$), implying highly unstable analyst workload. This instability persists across budgets and datasets, effectively disqualifying CADE from settings with fixed processing capacity. DeepDrebin, by contrast, maintains bounded variability ($\sigma[\text{Rej}]^* = 70–150$). Finally, temporal analysis reveals that several methods systematically deteriorate after deployment. Mann–Kendall trend estimates show that DeepDrebin improves over time on APIGraph ($\tau \approx 0.3–0.4$), while CADE variants exhibit consistent negative trends on Transcendent ($\tau < 0$). These effects are undetectable in single-shot evaluations but dominate long-horizon reliability. **In deployment reality, method selection rests on operational priorities that cannot be gleaned from in-lab F1 scores alone [1].** The multi-pillar evaluation of

AURORA makes these trade-offs explicit, embodying the paper’s central theme: when F1 becomes the target, it ceases to be a good measure of trustworthiness.

6 Limitations

Our active learning protocol uses uncertainty-based sample selection, which is common practice in malware detection [7, 44]. However, as noted by Arp et al. [1], sampling bias is a recognized pitfall in security ML: uncertainty sampling systematically selects non-representative samples near the decision boundary. While this approach has been effective for improving classification performance [7], future work should investigate whether alternative selection strategies (e.g., diversity sampling, stratified sampling) better serve the dual objectives of classification and calibration. Note that although we evaluated softmax alternatives for HCC and CADE, we retained each method’s original confidence function for active learning selection rather than testing softmax alternatives as selection criteria.

We omitted the Area Under Time (AUT) metric [32] as it essentially duplicates average metrics. We excluded the Population Stability Index (PSI) and the Prediction Accuracy Index (PAI) because they require separate development data splits and lack intuitive interpretability compared to our selected metrics. While the AURC provides valuable insights into confidence reliability across our evaluation, we acknowledge that, like all metrics, it comes with inherent tensions [39].

7 Conclusion

Our results challenge the prevailing SOTA paradigm in machine learning research for Android security: models are only as good as the metrics used to evaluate them. Rabanser and Papernot’s decomposition [35] identified ranking error as the critical bottleneck in selective classification; AURORA provides the empirical methodology to measure this bottleneck under the sustained distribution drift characteristic of malware detection. No single method consistently excels across all datasets and metrics. DeepDrebin tends to outperform more complex frameworks across confidence calibration, selective classification, and baseline performance. CADE exhibits severe reliability deficiencies with frequent miscalibration that undermines its core OOD detection premise. HCC provides superior temporal stability at lower budgets but suffers dramatic performance degradation at higher annotation budgets, questioning the value of both its computational complexity and the costly family labels. Interestingly, our findings suggest that added complexity may not translate to deployment robustness: the simplest neural approach (DeepDrebin) consistently outperforms SOTA frameworks while consuming a fraction of the computational budget and requiring no family labels.

Beyond proposing additional metrics, we advocate for a shift in security model evaluation that prioritizes multi-dimensional assessment over single-metric optimization, with particular emphasis on confidence reliability under drift. This holistic evaluation approach better reflects real-world security challenges where threats continuously evolve and would lead to more robust, deployable solutions than those optimized for accuracy under laboratory conditions. Ultimately, most models rely on the Drebin feature space [2],

which may be approaching saturation, suggesting future research should explore alternative feature representations to break through current performance plateaus.

8 Generative AI Usage

This work used generative AI tools for assistance with code development, literature review, and manuscript editing. All AI-generated content was reviewed and validated by the authors, who take full responsibility for the accuracy and integrity of the final submission.

References

- [1] Daniel Arp, Erwin Quiring, Feargus Pendlebury, Alexander Warnecke, Fabio Pierazzi, Christian Wressnegger, Lorenzo Cavallaro, and Konrad Rieck. 2022. Dos and Don'ts of Machine Learning in Computer Security. In *31st USENIX Security Symposium (USENIX Security 22)*. USENIX Association, 3971–3988.
- [2] Daniel Arp, Michael Spreitzenbarth, Malte Hubner, Hugo Gascon, and Konrad Rieck. 2014. DREBIN: Effective and Explainable Detection of Android Malware in Your Pocket. In *21st Annual Network and Distributed System Symposium, NDSS 2014, San Diego, California, USA, February 23–26, 2014*. The Internet Society. <https://www.ndss-symposium.org/ndss2014/drebin-effective-and-explainable-detection-android-malware-your-pocket>
- [3] AV-TEST. [n. d.]. *Malware Statistics and Trends Report*. <https://www.av-test.org/en/statistics/malware/> n. d.
- [4] Amin Azmoodeh, Ali Dehghantanha, and Kim-Kwang Raymond Choo. 2018. Robust malware detection for internet of (battlefield) things devices using deep eigenspace learning. *IEEE transactions on sustainable computing* 4, 1 (2018), 88–95.
- [5] Federico Barbero, Feargus Pendlebury, Fabio Pierazzi, and Lorenzo Cavallaro. 2022. Transcending Transcend: Revisiting Malware Classification in the Presence of Concept Drift. In *IEEE Symposium on Security and Privacy*.
- [6] Robert Bold, Haider Al-Khateeb, and Nikolaos Erselios. 2022. Reducing False Negatives in Ransomware Detection: A Critical Evaluation of Machine Learning Algorithms. *Applied Sciences* 12, 24 (2022), 12941.
- [7] Yizheng Chen, Zhoujie Ding, and David Wagner. 2023. Continuous Learning for Android Malware Detection. In *32nd USENIX Security Symposium (USENIX Security 23)*. USENIX Association, Anaheim, CA, 1127–1144. <https://www.usenix.org/conference/usenixsecurity23/presentation/chen-yizheng>
- [8] C Chow. 1970. On optimum recognition error and reject tradeoff. *IEEE Transactions on information theory* 16, 1 (1970), 41–46.
- [9] Charles Corbier, Nicolas Thome, Antoine Saporta, Tuan-Hung Vu, Matthieu Cord, and Patrick Perez. 2021. Confidence estimation via auxiliary models. *IEEE Transactions on Pattern Analysis and Machine Intelligence* 44, 10 (2021), 6043–6055.
- [10] Yukun Ding, Jinglan Liu, Jinjun Xiong, and Yiyu Shi. 2020. Revisiting the evaluation of uncertainty estimation and its application to explore model complexity-uncertainty trade-off. In *Proceedings of the IEEE/CVF Conference on Computer Vision and Pattern Recognition Workshops*. 4–5.
- [11] Ido Galil, Mohammed Dabbah, and Ran El-Yaniv. 2023. What can we learn from the selective prediction and uncertainty estimation performance of 523 imagenet classifiers. *arXiv preprint arXiv:2302.11874* (2023).
- [12] Yonatan Geifman and Ran El-Yaniv. 2017. Selective classification for deep neural networks. *Advances in neural information processing systems* 30 (2017).
- [13] Yonatan Geifman, Guy Uziel, and Ran El-Yaniv. 2019. Bias-Reduced Uncertainty Estimation for Deep Neural Classifiers. In *International Conference on Learning Representations*. <https://openreview.net/forum?id=SJfb5jCqKm>
- [14] Gen Digital Inc. (Norton). 2024. Act on quarantined risks or threats. <https://support.norton.com/sp/en-ie/home/current/solutions/v6200305>. Support article; accessed 06 Jun 2025.
- [15] Charles A. E. Goodhart. 1975. Monetary relationships: A view from Threadneedle Street. *Papers in Monetary Economics* 1 (1975).
- [16] Kathrin Grosse, Nicolas Papernot, Praveen Manoharan, Michael Backes, and Patrick McDaniel. 2017. Adversarial Examples for Malware Detection. In *Computer Security – ESORICS 2017*, Simon N. Foley, Dieter Gollmann, and Einar Snekkenes (Eds.). Springer International Publishing, Cham, 62–79.
- [17] Chuan Guo, Geoff Pleiss, Yu Sun, and Kilian Q. Weinberger. 2017. On calibration of modern neural networks. In *Proceedings of the 34th International Conference on Machine Learning - Volume 70* (Sydney, NSW, Australia) (ICML '17). JMLR.org, 1321–1330.
- [18] Md Ahsanul Haque, Md Mahmuduzzaman Kamol, Ismail Hossain, Suresh Kumar Amalapuram, Vladik Kreinovich, and Mohammad Saidur Rahman. 2025. CITADEL: A Semi-Supervised Active Learning Framework for Malware Detection Under Continuous Distribution Drift. *arXiv preprint arXiv:2511.11979* (2025).
- [19] William Hardy, Lingwei Chen, Shifu Hou, Yanfang Ye, and Xin Li. 2016. DL4MD: A deep learning framework for intelligent malware detection. In *Proceedings of the International Conference on Data Science (ICDATA)*. The Steering Committee of The World Congress in Computer Science, Computer . . ., 61.
- [20] Kilian Hendrickx, Lorenzo Perini, Dries Van der Plas, Wannes Meert, and Jesse Davis. 2024. Machine learning with a reject option: A survey. *Machine Learning* 113, 5 (2024), 3073–3110.
- [21] Dan Hendrycks and Kevin Gimpel. 2016. A baseline for detecting misclassified and out-of-distribution examples in neural networks. *arXiv preprint arXiv:1610.02136* (2016).
- [22] Dongkyoo Joo, Taesik Hong, and Ingoo Han. 2003. The neural network models for IDS based on the asymmetric costs of false negative errors and false positive errors. *Expert Systems with Applications* 25, 1 (2003), 69–75.
- [23] Roberto Jordaney, Kumar Sharad, Santanu K. Dash, Zhi Wang, Davide Papini, Ilya Nouretdinov, and Lorenzo Cavallaro. 2017. Transcend: Detecting Concept Drift in Malware Classification Models. In *26th USENIX Security Symposium*. USENIX Association, Vancouver, BC. <https://www.usenix.org/conference/usenixsecurity17/technical-sessions/presentation/jordaney> USENIX Sec.
- [24] Zeliang Kan, Feargus Pendlebury, Fabio Pierazzi, and Lorenzo Cavallaro. 2021. Investigating labelless drift adaptation for malware detection. In *Proceedings of the 14th ACM Workshop on Artificial Intelligence and Security*. 123–134.
- [25] Bojan Kolosnjaji, Apostolis Zarras, George Webster, and Claudia Eckert. 2016. Deep learning for classification of malware system call sequences. In *AI 2016: Advances in Artificial Intelligence: 29th Australasian Joint Conference, Hobart, TAS, Australia, December 5–8, 2016, Proceedings* 29. Springer, 137–149.
- [26] Henrik Linusson, Ulf Johansson, Henrik Boström, and Tuve Löfström. 2018. Classification with reject option using conformal prediction. In *Advances in Knowledge Discovery and Data Mining: 22nd Pacific-Asia Conference, PAKDD 2018, Melbourne, VIC, Australia, June 3–6, 2018, Proceedings, Part I* 22. Springer, 94–105.
- [27] Henry B. Mann. 1945. Nonparametric Tests Against Trend. *Econometrica* 13, 3 (1945), 245–259.
- [28] Enrico Mariconti, Lucky Onwuzurike, Panagiotis Andriotis, Emiliano De Cristofaro, Gordon Ross, and Gianluca Stringhini. 2016. Mamadroid: Detecting android malware by building markov chains of behavioral models. *arXiv preprint arXiv:1612.04433* (2016).
- [29] Jooyoung Moon, Jihyo Kim, Younghak Shin, and Sangheum Hwang. 2020. Confidence-aware learning for deep neural networks. In *international conference on machine learning*. PMLR, 7034–7044.
- [30] Mahdi Pakdaman Naeini, Gregory Cooper, and Milos Hauskrecht. 2015. Obtaining well calibrated probabilities using bayesian binning. In *Proceedings of the AAAI conference on artificial intelligence*, Vol. 29.
- [31] Annamalai Narayanan, Mahinthan Chandramohan, Lihui Chen, and Yang Liu. 2017. Context-aware, adaptive and scalable android malware detection through online learning (extended version). *arXiv preprint arXiv:1706.00947* (2017).
- [32] Feargus Pendlebury, Fabio Pierazzi, Roberto Jordaney, Johannes Kinder, and Lorenzo Cavallaro. 2019. TESSERACT: Eliminating Experimental Bias in Malware Classification across Space and Time. In *28th USENIX Security Symposium (USENIX Security 19)*. USENIX Association, Santa Clara, CA, 729–746. <https://www.usenix.org/conference/usenixsecurity19/presentation/pendlebury>
- [33] Feargus Pendlebury*, Fabio Pierazzi*, Roberto Jordaney, Johannes Kinder, and Lorenzo Cavallaro. 2019. TESSERACT: Eliminating Experimental Bias in Malware Classification across Space and Time. In *28th USENIX Security Symposium*. USENIX Association, Santa Clara, CA. USENIX Sec.
- [34] Xingzhi Qian, Xinran Zheng, Yiling He, Shuo Yang, and Lorenzo Cavallaro. 2025. LAMD: Context-driven Android Malware Detection and Classification with LLMs. *arXiv:2502.13055 [cs.CR]* <https://arxiv.org/abs/2502.13055>
- [35] Stephan Rabanser and Nicolas Papernot. 2025. What Does It Take to Build a Performant Selective Classifier? *arXiv preprint arXiv:2510.20242* (2025).
- [36] Joshua Saxe and Konstantin Berlin. 2017. eXpose: A character-level convolutional neural network with embeddings for detecting malicious URLs, file paths and registry keys. *arXiv preprint arXiv:1702.08568* (2017).
- [37] Glenn Shafer and Vladimir Vovk. 2008. A Tutorial on Conformal Prediction. *J. Mach. Learn. Res.* 9 (June 2008), 371–421.
- [38] Ben Sorscher, Robert Geirhos, Shashank Shekhar, Surya Ganguli, and Ari Morcos. 2022. Beyond neural scaling laws: beating power law scaling via data pruning. In *Advances in Neural Information Processing Systems*, Vol. 35. 19523–19536.
- [39] Jeremias Traub, Till J Bungert, Carsten T Lüth, Michael Baumgartner, Klaus H Maier-Hein, Lena Maier-Hein, and Paul F Jäger. 2024. Overcoming common flaws in the evaluation of selective classification systems. *Advances in Neural Information Processing Systems* 37 (2024), 2323–2347.
- [40] Trend Micro Service Central. 2023. Managing quarantine. <https://docs.trendmicro.com/en-us/documentation/article/cloud-app-security-online-help-managing-quarantine>. Online help page; accessed 06 Jun 2025.
- [41] VirusTotal. [n. d.]. *VirusTotal - Stats*. <https://www.virustotal.com/gui/stats> n. d..
- [42] Liyuan Wang, Xingxing Zhang, Hang Su, and Jun Zhu. 2024. A comprehensive survey of continual learning: Theory, method and application. *IEEE Transactions on Pattern Analysis and Machine Intelligence* (2024).

[43] Ke Xu, Yingjiu Li, Robert Deng, Kai Chen, and Jiayun Xu. 2019. Droidevolver: Self-evolving android malware detection system. In *2019 IEEE European Symposium on Security and Privacy (EuroS&P)*. IEEE, 47–62.

[44] Limin Yang, Wenbo Guo, Qingying Hao, Arridhana Ciptadi, Ali Ahmadzadeh, Xinyu Xing, and Gang Wang. 2021. CADE: Detecting and Explaining Concept Drift Samples for Security Applications. In *30th USENIX Security Symposium (USENIX Security 21)*. USENIX Association, 2327–2344. <https://www.usenix.org/conference/usenixsecurity21/presentation/yang-limin>

[45] Kim Zetter. 2014. *Countdown to Zero Day*. Crown, New York, NY, USA.

[46] Xiaohan Zhang, Yuan Zhang, Ming Zhong, Daizong Ding, Yinzheng Cao, Yukun Zhang, Mi Zhang, and Min Yang. 2020. Enhancing State-of-the-art Classifiers with API Semantics to Detect Evolved Android Malware. In *Proceedings of the 2020 ACM SIGSAC Conference on Computer and Communications Security (Virtual Event, USA) (CCS '20)*. Association for Computing Machinery, New York, NY, USA, 757–770. doi:10.1145/3372297.3417291

[47] Xu-Yao Zhang, Guo-Sen Xie, Xiali Li, Tao Mei, and Cheng-Lin Liu. 2023. A survey on learning to reject. *Proc. IEEE* 111, 2 (2023), 185–215.

[48] Xinran Zheng, Shuo Yang, Edith C. H. Ngai, Suman Jana, and Lorenzo Cavallaro. 2025. Learning Temporal Invariance in Android Malware Detectors. arXiv:2502.05098 [cs.CR]. <https://arxiv.org/abs/2502.05098>

[49] Fei Zhu, Zhen Cheng, Xu-Yao Zhang, and Cheng-Lin Liu. 2022. Rethinking confidence calibration for failure prediction. In *European conference on computer vision*. Springer, 518–536.

A Ethical Considerations

This work evaluates existing malware classifiers using publicly available datasets (APIGraph, AndroZoo, Transcendent) that have been widely used in prior peer-reviewed research [5, 7, 44, 46]. All datasets consist of aggregated application metadata and extracted features rather than raw user data, containing no personally identifiable information. Our research is purely evaluative – we propose no new attacks and our framework could not be repurposed to evade malware detection, as it assesses classifier reliability rather than exposing exploitable weaknesses. The selective classification approach we advocate would, if adopted, reduce harm by enabling classifiers to abstain on uncertain samples rather than producing confident misclassifications that could lead to false accusations (goodware flagged as malware) or missed threats (malware passing as benign). We see no direct ethical concerns arising from this work.

B Open Science Statement

This appendix enumerates all artifacts required to reproduce and evaluate the contributions of this paper, in accordance with CCS open science guidelines.

B.1 Artifacts Overview

Artifact	Description	Access
AURORA Framework	Evaluation framework code	Anonymous and standalone file
Experiment Scripts	Training & evaluation pipelines	Anonymous and standalone file
Config Files	Hyperparameters (App. D)	Anonymous and standalone file
Raw Results	Pickle files with predictions	Anonymous and standalone file
Datasets	APIGraph, AndroZoo, Transcendent	See below

B.2 Code and Scripts

The AURORA evaluation framework, including all experiment scripts, model implementations (Drebin, DeepDrebin, CADE, HCC), and

analysis notebooks, will be released under an open-source license. During double-blind review, the code is available at: <https://f003.backblazeb2.com/file/aurora-paper-and-artifacts/aurora-complete.zip>. The repository includes documentation for reproducing all experiments and figures presented in this paper.

B.3 Datasets

APIGraph and AndroZoo: We use the preprocessed datasets from Chen et al. [7], which extract Drebin-style features from Android APKs. These datasets are available at: https://drive.google.com/file/d/1O0upEcTolGyyvasCPkZFY86FNclk29XO/view?usp=drive_link.

Transcendent: We use the dataset from Barbero et al. [5], available at: <https://github.com/s2labres/transcendent-release?tab=readme-ov-file>.

C Algorithm for Post-Hoc Selective Classification

Algorithmic definitions of the *Post-Hoc Rejection Simulation* with associated subroutines for the single-value and class-specific uncertainty scores. The algorithm is designed to study the behavior of classifiers post-training under rejection. To perform this analysis, practitioners need to record the uncertainty scores S for every test month M_i in $\mathcal{D}_{\text{test}}$. In our evaluations, we experiment with rejection budgets of $\rho = \{0, 100, 200, \dots, 1500\}$ in steps of 100.

Algorithm 1 Post-hoc rejection routine

Require: Test stream $\mathcal{D}_{\text{test}} = \{M_1, \dots, M_N\}$, stored scores S_{M_i} , rejection quota ρ , method $\in \{\text{ood, softmax}\}$

- 1: $A \leftarrow S_{M_1}$ ▷ seed calibration pool
- 2: **for** $i = 2$ **to** N **do**
- 3: $S \leftarrow S_{M_i}$ ▷ scores for current month
- 4: $T \leftarrow i \times \rho$ ▷ samples to reject
- 5: **if** method == ood **then**
- 6: $c_i \leftarrow \text{ood_threshold}(A, T)$
- 7: **for all** $j \in M_i$ **with** $S[j] > c_i$ **do**
- 8: mark j as **rejected**
- 9: **end for**
- 10: **else** ▷ class-conditional soft-max
- 11: $(\ell_i, u_i) \leftarrow \text{softmax_thresholds}(A, T)$
- 12: **for all** $j \in M_i$ **with** $\ell_i \leq S[j] \leq u_i$ **do**
- 13: mark j as **rejected**
- 14: **end for**
- 15: **end if**
- 16: $A \leftarrow A \cup S$ ▷ update calibration pool
- 17: **end for**

D Hyperparameter Configurations

Drebin SVM. We conducted a search for the regularization parameter C from the set 0.001, 0.01, 0.1, 1, 10, 100, 1000. The best C is 1 for the Transcendent dataset, 0.1 for the APIGraph dataset, and 0.01 for the AndroZoo dataset.

DeepDrebin MLP. For the DeepDrebin implementation, we adhered to the configuration described in [16], employing a batch size of 512, Adam optimizer with default parameters, and a dropout

Algorithm 2 Class-conditional soft-max thresholds

```

1: function softmax_thresholds( $U, T$ )
2:   Input: uncertainty scores  $U$  (large  $\Rightarrow$  uncertain); quota
    $T$ 
3:   Output: lower / upper soft-max thresholds ( $\ell, u$ )
4:   sort  $U$  in descending order (most  $\rightarrow$  least uncertain)
5:    $\ell \leftarrow 1.0; u \leftarrow 0.0$ 
6:   for  $k = 0$  to  $T - 1$  do  $\triangleright$  take the  $T$  most-uncertain samples
7:      $v \leftarrow U[k]$ 
8:      $\ell \leftarrow \min(\ell, v); u \leftarrow \max(u, v)$ 
9:   end for
10:  return ( $\ell, u$ )  $\triangleright$  reject if  $\ell \leq p \leq u$ 
11: end function

```

Algorithm 3 Single-value uncertainty threshold

```

1: function ood_threshold( $U, T$ )
2:   Input: uncertainty scores  $U$ ; quota  $T$ 
3:   Output: cut-off  $c$  s.t. the  $T$  largest scores are rejected
4:   sort  $U$  in descending order
5:    $c \leftarrow U[T - 1]$   $\triangleright (T - 1)$  because of zero indexing
6:   return  $c$   $\triangleright$  reject if  $U > c$ 
7: end function

```

probability of $p = 0.5$. As part of our experimental design, we varied the number of epochs $e \in 30, 50$, though we found this choice to be relatively inconsequential, with $e = 30$ proving sufficient for convergence.

HCC. Our implementation mirrors the architecture and training protocol detailed in [7]. The encoder is a four-layer MLP that successively compresses the feature space through fully connected layers of sizes 512–384–256–128, each followed by ReLU activation, thus yielding a 128-dimensional embedding. The classifier adds two hidden layers with 100 ReLU units apiece and a final softmax over the two output neurons. We keep the mini-batch size at 1 024. For hyper-parameter selection in the *cold-start* phase, we explore the Cartesian product of two optimisers (SGD and Adam), four initial learning rates {0.001, 0.003, 0.005, 0.007}, three schedulers (cosine annealing without restart, step decay by a factor 0.95 every 10 epochs, and step decay by 0.5 every 10 epochs), and four training lengths {100, 150, 200, 250} epochs. In the subsequent *warm-start* phase, we further evaluate learning-rate scales {1 %, 5 %} of the initial value and either 50 or 100 additional epochs, again with both optimisers. The resulting best settings are as follows. For APIGRAPH, the cold-start model employs SGD with a learning rate of 0.003, step decay 0.95/10, and 250 epochs; during warm start we switch to Adam at 1.5×10^{-4} (i.e. 5 % of the initial rate) for 100 epochs after each monthly update. For ANDROZOO, the optimal cold-start uses SGD with a learning rate of 0.001, step decay 0.5/10, and 200 epochs; warm start then uses Adam at 1×10^{-5} (1 %) for 50 epochs. Finally, for TRANSCENDENT we obtain the best performance with SGD, a learning rate of 0.003, step decay 0.95/10, and 250 epochs, followed in warm start by Adam at 3×10^{-5} (1 %) for 100 epochs.

Note: Our HCC subsampling experiments employed stratified random sampling, which maintained the distribution of both binary and family labels in the reduced dataset.

CADE. We replicate the CADE setup in [7]: the OOD selector is paired with an MLP (cold and warm start) that mirrors the encoder dimensions in its decoder and shares the same classifier sub-network; batch size is 1 536, the MLP is trained for 50 epochs with a learning rate of 0.001, and we grid-search the autoencoder hyper-parameters (the original CADE study did not). For *cold start*, the optimal settings are APIGraph – Adam, lr 0.001 with step decay 0.95/10 epochs, 150 epochs; Androzoo – Adam, lr 0.001 with step decay 0.5/10 epochs, 100 epochs; and Transcendent – Adam, lr 0.003 with cosine decay, 100 epochs. For *warm start*, the best configurations are APIGraph – Adam, autoencoder lr 0.001 with cosine annealing for 250 pre-training epochs and, during active learning, lr reduced to 5 % of the initial value for both AE and MLP over 50 epochs; Androzoo – Adam, autoencoder lr 0.001 with cosine annealing for 100 epochs and lr scaled to 1 % during 50 active-learning epochs; and Transcendent – Adam, autoencoder lr 0.007 with step decay 0.95 over 200 epochs and, in the active phase, lr 0.00035 for 50 epochs.

E Initial Dataset Subsampling Investigation

This appendix presents an auxiliary investigation into whether cold-start training setups are inherently disadvantaged by treating the first year’s data (\mathcal{D}_0) as fully labeled while subsequent months contain far fewer labeled samples.

Research Question. Do Android malware classifiers suffer from an imbalance disadvantage due to an oversupply of training samples in the initial dataset \mathcal{D}_0 , compared to the sparsely labeled subsequent months?

E.1 Motivation and Methodology

Evaluating AURORA underscores an active learning tension: retaining knowledge in the extensive pool \mathcal{D}_0 versus adapting to drift in $\mathcal{D}_{\text{test}}$. Under a cold start, we posit that only a subset of \mathcal{D}_0 is beneficial. The B_{M_i} labels obtained each period convey the freshest drift signal, yet their gradient contribution may be outweighed by the abundance of historical samples, diverting optimization toward outdated patterns. We denote $B_0 \subseteq \mathcal{D}_0$ as the initial training budget.

To illustrate the magnitude of this imbalance, we examine the Transcendent dataset [5]. It contains 57,740 samples in its first year. A monthly test budget of $B_{M_i} = 50$ adds only 0.1 % to the initial pool \mathcal{D}_0 and grows to merely 4.1 % after the 48 months of the test set. We analyze whether the pronounced ratio $B_{M_i} \ll \mathcal{D}_0$ restricts the adaptation to emerging malware and study how subsampling \mathcal{D}_0 influences the performance of the downstream classifier. We explore two subsampling schemes:

- **StratK-Sampling.** Stratified random draws that preserve the binary label ratio of the pool.
- **Uncertainty-Sampling.** Selection of the B_{M_i} instances with the highest predictive uncertainty, reflecting drift-aware practice in malware classification where such samples most effectively refine the decision boundary.

We vary the initial-budget B_0 to assess how much of \mathcal{D}_0 is actually required. The values are anchored in prior work [7, 44]: with a 12-month training horizon, $B_0 = 12$ corresponds to “one selected obs/month”, and $B_0 = 4800$ equals “400 obs/month.” Each configuration is paired with a monthly label-budget $B_{M_i} \in \{50, 100, 200, 400\}$.

All experiments use DeepDrebin for 30 training epochs. Every combination of B_0 and B_{M_i} is run five times on each of the three datasets. For *Uncertainty-Sampling* we partition \mathcal{D}_0 into $k = 6$ folds, train on $k - 1$ folds, and, from the held-out fold, retain the $\frac{B_0}{k}$ instances with the highest predictive uncertainty; concatenating the selections across folds yields the desired subset.

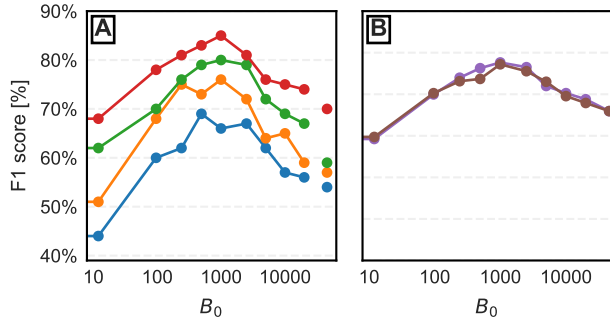


Figure 4: Continuous-learning performance of DeepDrebin (with cold-start) on the *androzoo* benchmark. **A** shows the effect of four monthly label-budget settings ($B_{M_i} = 50$, $B_{M_i} = 100$, $B_{M_i} = 200$, $B_{M_i} = 400$) over increasing amounts of initially-labeled data B_0 . **B** contrasts two subsampling heuristics applied to the initial pool \mathcal{D}_0 —**StratK-Sampling** and **Uncertainty-Sampling**—with results averaged across all label-budget settings to allow direct comparison. Horizontal dashed lines mark 10-percentage-point intervals; both panels share the same 40–90 % F_1 -score range and use a logarithmic x -axis.

The results are summarized in Figure 4. We plot the F1 against the initial-budget B_0 ; the rightmost point corresponds to training on $B_0 = \mathcal{D}_0$. Increasing the monthly budget B_{M_i} improves F1, most notably on the Androzoo dataset. *Uncertainty-Sampling* has no advantage over *StratK-Sampling*, implying that label-balanced random draws suffice.

Connection to Data Pruning Literature. Our observation that subsampling \mathcal{D}_0 can improve performance is consistent with recent work on data pruning in deep learning. Sorscher et al. [38] demonstrated that strategic data selection can outperform power-law scaling, particularly when data diversity is more important than sheer quantity for generalization. In the context of concept drift, historical data from \mathcal{D}_0 may contain patterns that no longer reflect current malware behavior. By subsampling, we implicitly reduce the influence of potentially outdated patterns while preserving diversity across the initial training period. This may partially explain the counter-intuitive finding that *less* data can yield *better* adaptation to drift, though we note that the precise mechanisms warrant further investigation.

E.2 Insights

In Table 1, we observe that subsampling of \mathcal{D}_0 either produces gains in F1 and AURC (Androzoo) or maintains stability with negligible changes (APICGraph and Transcendent), confirming that reducing B_0 can enhance both performance and uncertainty calibration without adverse effects across cold-start configurations.

In Androzoo, subsampling with $B_0 = 4800$ shows mixed effects across methods and budgets. DeepDrebin achieves consistent gains of +17, +17, +22, +14 at $B_{M_i} = 50, 100, 200, 400$ respectively. HCC shows mixed effects with minimal changes (−3, +3, +4, 0). Drebin with $B_0 = 4800$ reports gains at the lowest budget (+6% at $B_{M_i} = 50$) while maintaining comparable performance at higher budgets. In both APICGraph and Transcendent datasets, $B_0 = 4800$ maintains performance stability across the varying B_{M_i} .

Subsampling the initial dataset \mathcal{D}_0 leads to substantial AURC benefits on Androzoo, while having negligible effects on APICGraph and Transcendent. DeepDrebin with $B_0 = 4800$ shows significant AURC improvements on Androzoo (−3.9, −4.7, −4.7, −2.9 at $B_{M_i} = 50, 100, 200, 400$ respectively), while HCC shows slight improvements (−0.2, 0, −0.2, −0.2).

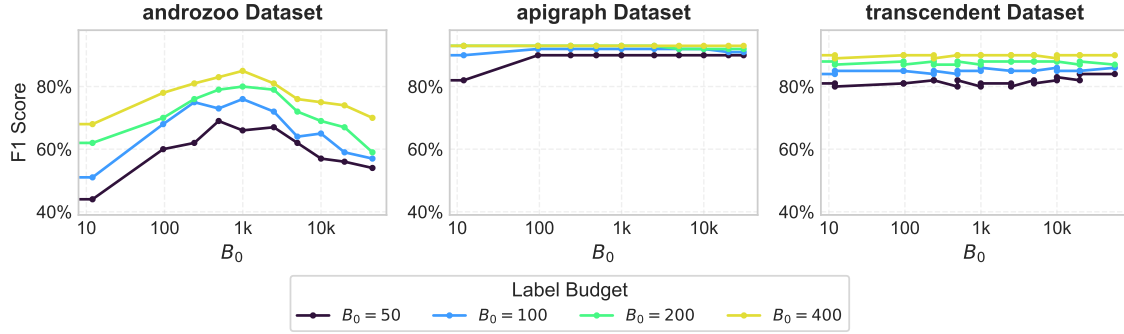


Figure 5: Results for *Uncertainty-Sampling*. Average Performance across $n = 5$ trials with *DeepDrebin* on selected datasets. For every B_{M_i} (monthly label budget for $\mathcal{D}_{\text{test}}$) and B_0 (selected samples from \mathcal{D}_0) we run a full experiment on the all months in $\mathcal{D}_{\text{test}}$ and report the average monthly performance, excluding the first 6 months of the test-period as per standard-protocol [7, 44].

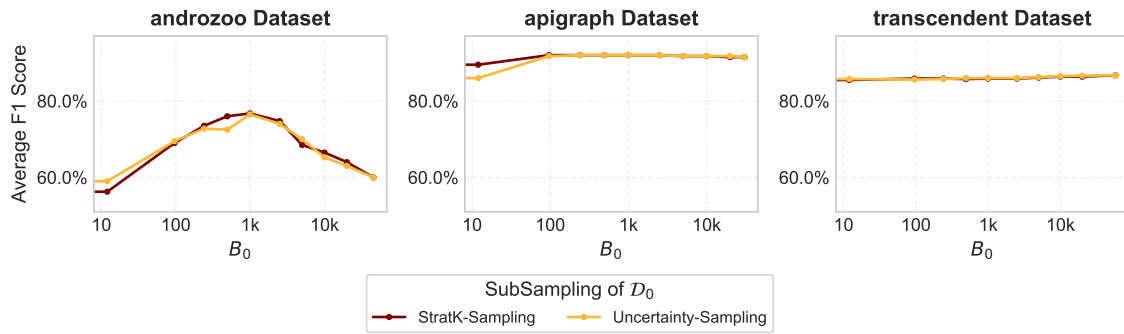


Figure 6: Comparison of *Uncertainty-Sampling* and *StratK-Sampling*. Results are additionally averaged across all B_{M_i} 's to allow for a direct comparison. We find that *StratK-Sampling* is on par with *Uncertainty-Sampling*.